J. Phys. B: At. Mol. Opt. Phys. **33** (2000) 4833–4848. Printed in the UK PII: S0953-4075(00)51215-2

Threshold photoelectron studies of Kr and Xe

A E Slattery†, J P Wightman†, M A MacDonald‡, S Cvejanović† and T J Reddish†

† Physics Department, The University of Newcastle, Newcastle upon Tyne NE1 7RU, UK
‡ CLRC, Daresbury Laboratory, Daresbury, Warrington WA4 4AD, UK

Received 4 July 2000

Abstract. Threshold photoelectron measurements of the ionic 'satellite' states of krypton and xenon have been undertaken at the Daresbury Synchrotron Radiation Source (SRS) using the field-penetration technique. The photon energy ranges covered were 27.5–32.3 eV (Kr) and 23.3–34.8 eV (Xe) with a measured energy resolution of 13 meV, which is an order of magnitude improvement over the previous measurements. The ionic states have been catalogued and where resonance enhancement has been observed, the corresponding doubly excited neutral states have also been identified.

1. Introduction

The photoionization of atoms can produce excited ionic states as well as the dominant 'single-hole' ion states. The presence of these excited states, often referred to as 'satellite' or 'correlation' states, has prompted studies of their excitation mechanisms from measurements of their partial cross sections and the angular dependence of the ejected electron. These kinds of measurements are in addition to the basic spectroscopy where one desires to accurately determine—both experimentally and theoretically—the ionic state energies and assign them using appropriate angular momentum coupling schemes.

Threshold photoelectron spectroscopy (TPES) is one method that has been previously limited solely by the photon resolution. This type of spectroscopy is generally associated with the field-penetration technique, whereby one uses a static electric field to extract over 4π sr electrons of energies smaller than a certain value (Cvejanović and Read 1974). With a bandwidth, ΔE, of typically ~ 5 meV, TPES determines the partial cross sections of all the states at their threshold on the same intensity scale. The high efficiency of the method is a great asset in detecting the many excited ionic states that have small cross sections. The disadvantages, however, are that information on the electron emission angles (measured with respect to the polarized light source) is lost and the partial cross sections over an extended range of electron energies cannot be achieved. Nevertheless, this technique complements other photoelectron spectroscopy (PES) methods that provide that insight.

One of the peculiarities of TPES is that virtually every ionic state is observed. In the case of Kr^+ and Xe^+, the subjects of this study, both quartet and doublet ion states are readily observed—in contrast with measurements at higher photon energies where the dipole-allowed doublet states (e.g. ^2S, ^2P) dominate. This observation is generally associated with interchannel coupling (IC), which takes into account both the interactions with continuum states (continuum state configuration interaction, CSCI) and with those doubly excited discrete states (resonances) which lead to autoionization (see, for example, Becker and Shirley 1990, Kikas *et al* 1996):

$$\begin{array}{lll} h\nu + \mathrm{A} \longrightarrow & \mathrm{A}^{+*} + \mathrm{e}^- & \text{direct ionization} \\ \quad\searrow \quad \nearrow & & \\ \quad\;\; \mathrm{A}^{**} & & \text{indirect ionization.} \end{array}$$

The presence of neutral states that couple to the ionization continuum in this manner has been long known to be a significant photoionization mechanism in the near-threshold region of a particular state. The excitation functions of the prominent single-hole states display strong interference profiles arising from the mixing of the direct and indirect photoionization routes. In contrast, quartet states have no, or little, direct cross section so the indirect process leads to symmetric peaks in their excitation functions. Although CSCI is generally more important towards threshold, the partial cross section *at* threshold will depend largely on the cross sections of the nearest resonance states and the strength of the coupling to them. The presence of resonances can often be inferred from large relative intensity variations within members of a multiplet and, more directly, by the existence of shoulders or small peaks on the high-energy side of the threshold peak (see, for example, Cvejanović *et al* 1994†). Consequently, although TPES is essentially the spectroscopy of ionic states, certain excited neutral states can also be observed. Conventional PES techniques (e.g. 'constant ionic state' (CIS) measurements) are able to focus on the interplay between resonant and direct excitation of ionic states. However, non-trivial experimental problems in controlling the electron analyser transmission function in the low-energy range have to be solved.

Recent PES studies of Kr and Xe have been measured by Kikas *et al* (1996) with 88 and 63.5 eV photons, respectively, the corresponding energy resolutions being 73 and 61 meV, respectively. Whitfield *et al* (1994) and Lagutin *et al* (1996) used a number of photon energies in the 40–150 eV range in their time-of-flight PES study of Xe, having an energy resolution of 86–135 meV, depending on the electron energy. The theoretical and experimental study of Lagutin *et al* (1996) also reviewed the overall progress made in understanding the electron angular distributions and partial cross sections of these states in comparison with the Xe^+ 5s $^2S_{1/2}$ state. These studies build on earlier work by Svensson *et al* (1988), Krause *et al* (1992), Wills *et al* (1990) and Carlsson-Göthe *et al* (1991), the latter being the highest resolution PES study to date (50 meV) obtained using He II radiation (40.8 eV). Further complementary theoretical and experimental studies in Kr have been provided by measuring absolute partial cross sections for a number of ionic states using photon-induced fluorescence spectroscopy (PIFS) (see Schmoranzer *et al* 1993, Lagutin *et al* 1994, Ehresmann *et al* 1994, Sukhorukov *et al* 1995 and references therein).

Recently, very high-resolution pulsed-field ionization zero kinetic energy (PFI-ZEKE) photoelectron spectroscopy has been performed on xenon by Shiell *et al* (1998, 1999) at the Advanced Light Source (ALS). This elegant technique field-ionizes (in the dark period between synchrotron light pulses) the long-lived, very high-*n* Rydberg states just *below* the series limit which corresponds to an ionic state, and detects the liberated electron with an overall resolution of $<$1 meV.

$$h\nu + \mathrm{A} \rightarrow \mathrm{A}^{**} \rightarrow \mathrm{A}^{*+} + \mathrm{e}^- \qquad \text{PFI-ZEKE.}$$

Consequently, this detection method is virtually insensitive to the nearby, shorter-lived, doubly excited neutral states that converge to *higher*-energy ionic states. Their studies were restricted to the 11 Xe^+ states below 25 eV.

† Similar resonance features have also been observed in electron impact threshold spectroscopy (for example, see Jureta *et al* 1978).

In this work, TPES was used to investigate the ionic states of krypton and xenon, building on our earlier work in argon (Cvejanović *et al* 1994). The previous TPES study of Kr and Xe by Hall *et al* (1990) had a photon resolution of about 100 and 75 meV, respectively. The present work was undertaken using the same bending magnet beamline on a second-generation synchrotron source (SRS-3.3). Nearly 120 ionic states below 35 eV in Xe were observed along with over 30 below 32 eV in Kr. As such, this study sets a baseline from which further progress made on third-generation sources can be judged.

2. Experimental

Apparatus originally designed for photoelectron–photoelectron coincidence studies (Reddish *et al* 1997) was used as a threshold photoelectron spectrometer in conjunction with a toroidal grating monochromator (TGM) at the Daresbury SRS. The spectrometer consists of two toroidal analysers configured to detect electrons emitted in a plane orthogonal to the incoming photon beam. In this threshold work, an adaptation of the penetrating-field technique was used to extract efficiently and selectively near-zero energy electrons, which were then detected after passing through one of the energy analysers. The details of the electron optical arrangement have been given in Cvejanović *et al* (1994) and since then minor changes have been made to the entrance lens which result in about a factor of three greater rejection of the characteristic high-energy tail.

The measured FWHM of the threshold peaks is typically $\sim$13 meV, which is a combination of the photon resolution and the sharply peaked, but asymmetric, threshold analyser response function. The high photon resolution was obtained by operating the beamline optics in a way that minimized the aberrations over the photon energy range covered in this experiment. Unlike an earlier argon study (see Cvejanović and Reddish 1995), a determination of the analyser efficiency function was not attempted in this work.

The threshold spectra shown in figures 1–3 are composed of separate scans in fixed energy steps of 5 meV and an accumulation time of 5 s/point over (typically) 2 eV long sections of the photon energy scale. Each new section had substantial regions of overlap with the previous one. The photon flux was continuously monitored using an aluminium photodiode, which enabled us to normalize the spectra for variations in the photon flux both within a section and between them. The photon energy scale was calibrated and its linearity checked by using a range of prominent ionic states in conjunction with well established spectroscopic energies (Moore 1952, 1958, Minnhagen *et al* 1968, Hansen and Persson 1987).

An aluminium filter was not employed in these experiments and consequently there is a possibility of contamination due to second- (or third-) order output from the monochromator. This would result in photons of double (or triple) the energy value also being present at the interaction region, but with significantly reduced intensity. This could be troublesome for these targets due to the strong shake-off inner-shell resonances, converging to the $Kr(3d_{5/2,3/2})^{-1}$ and $Xe(4d_{5/2,3/2})^{-1}$ states, which couple to the double-ionization continuum and so can result in threshold electrons (see Heimann *et al* 1987, Avaldi *et al* 1991). Evidence for this process at the appropriate photon energies will be discussed in the next section.

3. Results and discussion

The general overviews of the threshold photoelectron spectrum for krypton and xenon are shown in figures 1 and 3. Both spectra begin with the $4s4p^6$ and $5s5p^6$ $^2S_{1/2}$ single-hole states at 27.511 and 23.397 eV, respectively, omitting the main lines, $4s^24p^5$ and $5s^25p^5$ $^2P_{1/2,3/2}$,

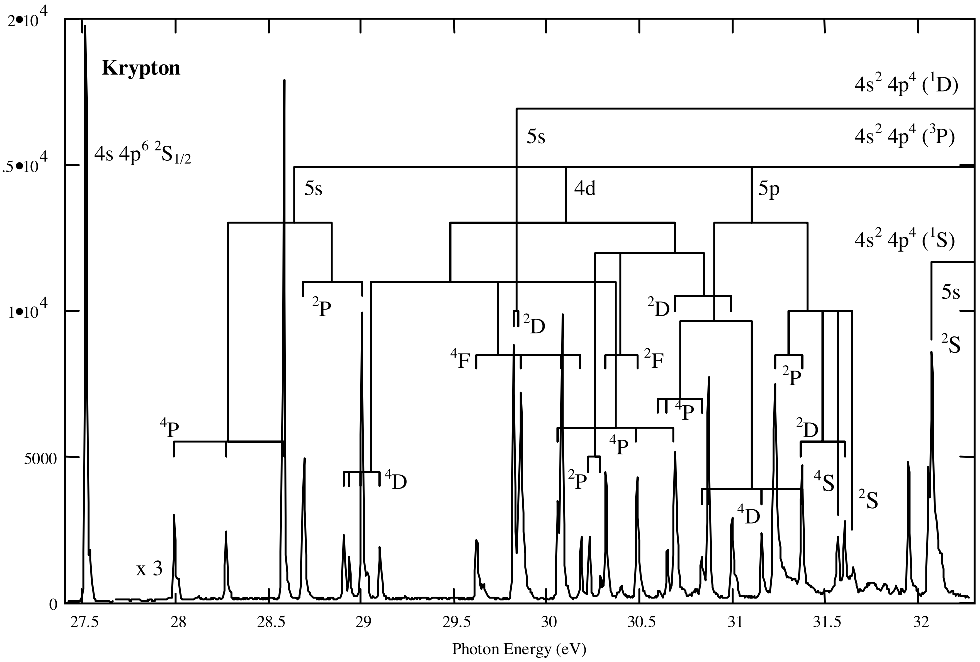

Figure 1. The threshold photoelectron spectrum of krypton with spectroscopic assignments based on Minnhagen *et al* (1968).

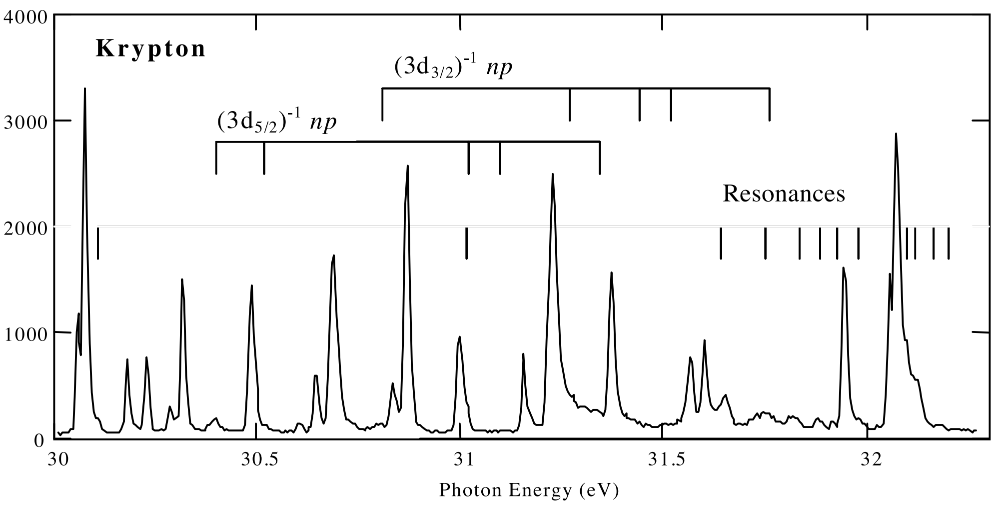

Figure 2. An expanded view of the TPES of krypton between 30 and 32.2 eV. The positions of the observed resonances listed in table 2 are indicated and the assignment bars show the positions of the possible threshold features arising from third-order light, as discussed in the text.

at lower energies. In general, only a few krypton states show clear evidence of resonance excitation on the high-energy side of the threshold peaks, with very little evidence in the case of xenon. The identified ionic states are listed in tables 1 and 3 and the measured energies

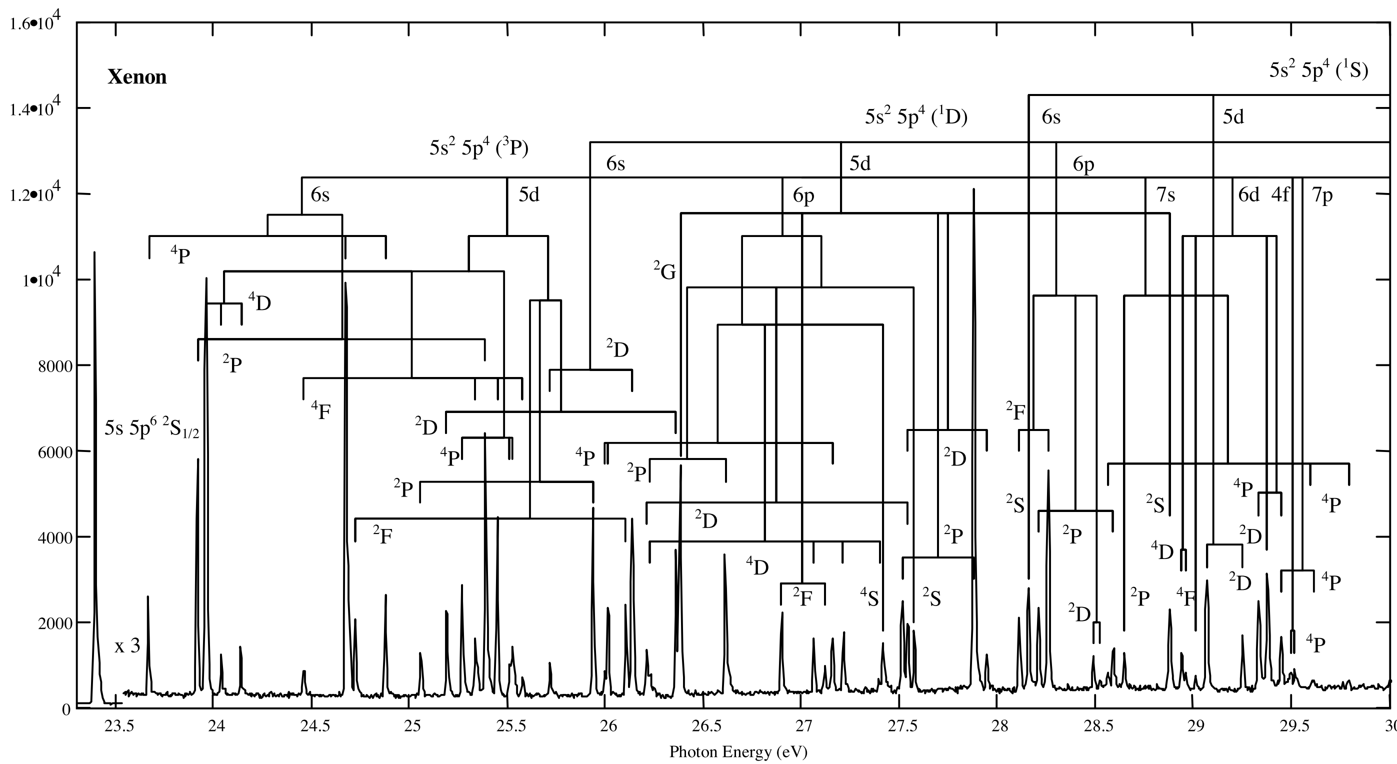

Figure 3. The threshold photoelectron spectrum of xenon with spectroscopic assignments from Hansen and Persson (1987). Note that above ∼28.5 eV not all of the multiplet members have been observed (see table 3 for details).

have an average deviation from the optical studies of <1 meV across the entire energy range. Although the LS-coupling scheme is commonly used to designate the states, it is widely recognized that in such heavy ions this coupling scheme is adequate rather than rigorous. Indeed, Hansen and Persson (1987) also give the jK designation for all the Xe^+ states and closer to the double-ionization thresholds the LS-coupling scheme is abandoned in both Xe^+ and Kr^+ (see also Minnhagen *et al* 1968). Ionic states with high total angular momenta of $J = \frac{5}{2}, \frac{7}{2}$ and $\frac{9}{2}$ are clearly identified, implying a correspondingly high-ℓ value for the partial wave of the continuum electron. It is also worth noting that although the majority of observed satellite states have even parity, odd-parity states are also seen, as they were in earlier PES studies. The original assignments (see Moore 1952, 1958) of the ionic states in the energy regions covered in the spectra are broadly uncontested. However, there are a few states whose assignments—or ordering—were questioned in the previous studies, as indicated in the tables and discussed in the following sections. The spectroscopic bars in figures 1 and 3 follow the assignments of the more recent optical studies by Minnhagen *et al* (1968) and Hansen and Persson (1987) for krypton and xenon, respectively. Unfortunately, TPES alone cannot resolve the question of assignment as further experimental information, such as β parameter trends, is required. However, this needs similarly high-resolution PES studies in order to resolve the states and presently such measurements are not available. Nevertheless, the improved resolution in this study has resolved many multiplet states into their various members for the first time using photoelectron detection methods.

3.1. Krypton

The most intense satellite state in the threshold spectrum is $(^3P)5s\ ^4P_{1/2}$ at 28.576 eV. This feature, which is significantly more intense than other members of the same multiplet, has probably been influenced by the nearby $(^1D)5s\ ^2D_{5/2}$ 6p neutral state. Lagutin *et al* (1994) have shown that this Rydberg series of resonances not only strongly interferes with the $4s4p^6$ $^2S_{1/2}$ state, but also enhances the $(^3P)5s\ ^4P$ states at *higher* photon energies. As such this is an example where the ion core changes state (and so is not a spectator) during the resonance decay process. As mentioned earlier, shoulders on the high-energy side of threshold peaks are direct evidence of resonance decay. Table 2 lists the observed features of that kind and, where known, the resonant assignments. Below 31 eV, the presence of the $(^3P)5s\ ^2P_{1/2}$ 6p state at 27.54 eV, which decays to the $^2S_{1/2}$ single-hole state, and the $(^1D)4d\ ^2D_{3/2}$ 5p state at ~ 29.64 eV, which decays to $(^3P)4d\ ^4F_{9/2}$, are arguably the clearest features observed (see figure 1). One again notes that the ion core changes state during the decay together with the coupling between spin and orbital angular momenta of the outer electrons that also results in an odd-parity partial wave for the free electron.

Most of the ionic states observed in this study have been identified and assigned by optical methods (see table 1), but there are a few notable discrepancies in the assignment of some of the states, namely those states associated with the $(^3P)4d$ configuration. Minnhagen *et al* (1968) re-assigned two states at ~ 30.25 eV to the $(^3P)4d\ ^2P$ doublet, which is supported by PES studies as the doublet states generally dominate the photoelectron spectrum away from threshold. Sukhorukov *et al* (1995), however, suggest the 4d $^2P_{1/2,3/2}$ states are at 30.06 and 30.49 eV, respectively. Both Minnhagen *et al* (1968) and Sukhorukov *et al* (1995) suggest a much larger splitting for the low-J values of the $(^3P)4d\ ^4F$ multiplet and a smaller splitting for the $(^3P)4d\ ^2F$ states compared with those of Moore (1952), but differ on the precise energy of the $^2F_{5/2}$ component. Minnhagen *et al* (1968) also reassigns the $(^3P)4d\ ^4P$, ^2D multiplet members to other observed energies. It is also likely that a lack of resolution on earlier synchrotron studies hampered the assignment of these satellite states.

Table 1. The energies and assignments of the ionic states in krypton between 27.5 and 32.1 eV.

	This work	Moore (1952)		Minnhagen *et al* (1968)		Sukhorukov *et al* (1995)	
	Energy (eV)	Energy (eV)	Assignment	Energy (eV)	Assignment[b]	Energy (eV)	Assignment[b]
1	27.511[a]	27.5105	$4p^6 4s\ {}^2S_{1/2}$			27.51	
2	27.988[a]	27.9851	$({}^3P)5s\ {}^4P_{5/2}$			27.99	
3	28.267	28.2658	$({}^3P)5s\ {}^4P_{3/2}$			28.27	
4	28.576	28.5771	$({}^3P)5s\ {}^4P_{1/2}$			28.58	
5	28.684	28.6852	$({}^3P)5s\ {}^2P_{3/2}$			28.69	
6	28.901	28.9003	$({}^3P)4d\ {}^4D_{7/2}$			28.90	
7	28.929	28.9272	$({}^3P)4d\ {}^4D_{5/2}$			28.93	
8	28.999[a]	28.9986	$({}^3P)5s\ {}^2P_{1/2}$			29.00	
		28.9983	$({}^3P)4d\ {}^4D_{3/2}$			29.00	
9	29.094	29.095	$({}^3P)4d\ {}^4D_{1/2}$			29.10	
10	29.617[a]	29.6183	$({}^3P)4d\ {}^4F_{9/2}$			29.62	
11	29.815	29.8163	$({}^1D)5s\ {}^2D_{3/2}$			29.82	
12	29.852	29.8574	$({}^1D)5s\ {}^2D_{5/2}$			29.86	
		29.8490	$({}^3P)4d\ {}^4F_{7/2}$				
13	30.055			30.0588	$({}^3P)4d\ {}^4P_{1/2}$	30.06	$({}^3P)4d\ {}^2P_{1/2}$
14	30.077[a]	30.0766	$({}^3P)4d\ {}^4F_{5/2}$			30.08	
		30.0821	$({}^3P)4d\ {}^4F_{3/2}$				
15	30.177	30.1777	$({}^3P)4d\ {}^4P_{1/2}$	30.1775	$({}^3P)4d\ {}^4F_{3/2}$	30.18	$({}^3P)4d\ {}^4F_{3/2}$
16	30.225	30.2249	$({}^3P)4d\ {}^4P_{3/2}$	30.2247	$({}^3P)4d\ {}^2P_{1/2}$	30.23	$({}^3P)4d\ {}^4P_{1/2}$
17	30.284	30.2847	$({}^3P)4d\ {}^4P_{5/2}$	30.2844	$({}^3P)4d\ {}^2P_{3/2}$	30.29	$({}^3P)4d\ {}^4P_{3/2}$
18	30.316	30.3165	$({}^3P)4d\ {}^2F_{7/2}$			30.32	
19	30.482	30.4818	$({}^3P)4d\ {}^2D_{3/2}$	30.4816	$({}^3P)4d\ {}^4P_{3/2}$	30.49	$({}^3P)4d\ {}^2P_{3/2}$
				30.4822	$({}^3P)4d\ {}^2F_{5/2}$		$({}^3P)4d\ {}^4P_{5/2}$
20	30.599	30.6007	$({}^3P)5p\ {}^4P^o_{5/2}$			30.60	
21	30.645	30.6456	$({}^3P)5p\ {}^4P^o_{3/2}$			30.65	
22	30.682[a]	30.6804	$({}^3P)4d\ {}^2D_{5/2}$	30.6801	$({}^3P)4d\ {}^4P_{5/2}$	30.68	$({}^3P)4d\ {}^2F_{5/2}$
				30.6869	$({}^3P)4d\ {}^2D_{3/2}$		
23	30.832	30.8309	$({}^3P)5p\ {}^4P^o_{1/2}$			30.83	
		30.8309	$({}^3P)5p\ {}^4D^o_{7/2}$				
24	30.864	30.8666	$({}^3P)5p\ {}^4D^o_{5/2}$				
25	30.993[a]	30.9941	$({}^3P)4d\ {}^2F_{5/2}$	30.9940	$({}^3P)4d\ {}^2D_{5/2}$		
26	31.152	31.1531	$({}^3P)5p\ {}^4D^o_{3/2}$				
27	31.224	31.2426	$({}^3P)5p\ {}^2P^o_{1/2}$				
28	31.367	31.3685	$({}^3P)5p\ {}^2D^o_{5/2}$				
		31.3707	$({}^3P)5p\ {}^2P^o_{3/2}$				
		31.3740	$({}^3P)5p\ {}^4D^o_{1/2}$				
29	31.564	31.5673	$({}^3P)5p\ {}^4S^o_{3/2}$				
30	31.598	31.6012	$({}^3P)5p\ {}^2D^o_{3/2}$				
31	31.645[a]	31.6468	$({}^3P)5p\ {}^2S^o_{1/2}$				
32	31.944[a]		[b]				
33	32.053		[b]				
34	32.073[a]	32.0745	$({}^1S)5s\ {}^2S_{1/2}$				

[a] Resonance observed on the high-energy side of the threshold peak (see table 2).
[b] Where different from that of Moore (1952).
[c] Previously unassigned, possibly the 'missing' $({}^1D)4d\ {}^2G$ or ${}^2F$ states.

The 31.2–32.2 eV region of the threshold spectrum in figure 2 seems strange as the threshold yield above the odd-parity $({}^3P)5p\ {}^2P$ state at 31.224 eV does not return to the

Table 2. Observed resonances in the threshold photoelectron spectrum of krypton of figure 1.

This work Energy (eV)	Codling and Madden (1972) Energy (eV)	No	Assignment
27.54	27.542	36	$(^3P)5s\ ^2P_{1/2}\ 6p$ [b]
28.01			
29.03 [a]	29.026	45	
29.64 [a]	29.638	62	$(^1D)4d\ ^2D_{3/2}\ 5p$ [b]
29.66	29.664	63	
30.11			$(^1D)4d\ ^2S_{1/2}\ 5p$? [b]
30.73	30.739	76	
31.02 [a]	31.016	79	
31.65	31.642	85	
31.75	31.751	87	$(^1S)5s\ ^2S_{1/2}\ 9p$ [c]
31.82	31.833	89	$(^1S)5s\ ^2S_{1/2}\ 10p$ [c]
31.88 [a]	31.886	90	$(^1S)5s\ ^2S_{1/2}\ 11p$ [c]
31.91 [a]	31.925	91	$(^1S)5s\ ^2S_{1/2}\ 12p$ [c]
31.98			
32.10	32.099	97	
32.12 [a]			
32.19 [a]	32.166	98	
	32.201	99	$(^1D)4d\ ^2D_{5/2}\ 9p$

[a] Resonance also observed by Hall *et al* (1990) in the partial photoionization cross sections of selected satellite states.
[b] Assignment from Lagutin *et al* (1994). That study also finds a series of resonances between 30.8 and 31.6, and one at ~ 32.1 eV.
[c] Rydberg series based on Kr^+ $(^1S)5s\ ^2S_{1/2}$ at 32.078 eV.

'baseline' for at least 0.2, or more, eV. The observed shape contains what appears like a continuum between 31.25 and 31.5 eV, superimposed with another sharp threshold feature at 31.367 eV (see table 1). This is so atypical of threshold spectra that one might consider this enhanced sensitivity at the end of this spectrum to be an experimental artefact. However, immediately after this scan, other threshold spectra were taken at lower photon energies that confirmed the earlier measurements presented here, implying a constancy in the threshold analyser tuning conditions. We note, however, that this region of the spectrum would correspond to the energy range of the previously mentioned $Kr(3d^{-1})np$ shake-off resonances which could be excited by third-order light and produce threshold electrons. On closer examination there are unidentified weak peaks at 30.40 and 30.80 eV which would correspond to the $Kr(3d_{5/2,3/2})^{-1}5p$ states at 91.20 and 92.43 eV, respectively (Heimann *et al* 1987). The 91.2 eV state is the most intense of the series and so indicates the level of third-order contamination, making the not unreasonable assumption that its contribution is uniform in the limited 30.4–31.7 eV photon energy range. It should also be noted that the $Kr(3d_{5/2,3/2})^{-1}$ series limits are shifted upwards in energy by ~ 240 meV, due to post-collisional interaction (PCI), and have natural linewidths of $\sim$100 meV (see Avaldi *et al* 1991, Čubrić *et al* 1992 and references therein). Despite the two $Kr(3d_{5/2,3/2})^{-1}5p$ peaks, no other features of significant intensity are discernible in the spectrum. Consequently, it is highly unlikely that the third-order light contamination causes the observed effect.

Given the peak shape of the lower threshold peaks, it seems more likely that the observed continuum-like 'tail' between 31.25 and 31.5 eV is due, at least in part, to resonances even though no structure is discernible. Calculations by Lagutin *et al* (1994) (see their figure 5) also indicate a series of resonances between 30.8 and 31.6 eV (and at ~ 32 eV too), which

Table 3. The energies and assignments of the ionic states in xenon between 23.3 and 30.0 eV.

	This work	Hansen and Persson (1987)		Carlsson-Göthe *et al* (1991)	Kikas *et al* (1996)	Hall *et al* (1990)	Shiell *et al* (1999)
	Energy (eV)	Energy (eV)	Assignments	Energy (eV)	Energy (eV)	Energy (eV)	Energy (eV)
1	23.393	23.397	$5s5p^6\ ^2S_{1/2}$	23.397	23.40	23.397	23.3967
2	23.664	23.669	$(^3P)6s\ ^4P_{5/2}$	23.658		23.66	23.6689
3	23.912	23.917	$(^3P)6s\ ^2P_{3/2}$	23.919	23.92		23.9164
4	23.957	23.958	$(^3P)5d\ ^4D_{5/2}$	23.958		23.95	23.9576
		23.963	$(^3P)5d\ ^4D_{7/2}$	23.962			23.9627
5	24.035[a]	24.037	$(^3P)5d\ ^4D_{3/2}$	24.038			24.0366
6	24.137[a]	24.139	$(^3P)5d\ ^4D_{1/2}$	24.139		24.13	24.1388
7	24.456	24.455	$(^3P)5d\ ^4F_{9/2}$	24.450	24.46	24.45	24.4546
8	24.671[a]	24.672	$(^3P)6s\ ^4P_{1/2}$	24.672	24.67	24.67	24.6719
9	24.719	24.719	$(^3P)5d\ ^2F_{7/2}$	24.719			24.7188
10	24.875	24.876	$(^3P)6s\ ^4P_{3/2}$	24.876	24.86	24.86	24.8754
11	25.055	25.055	$(^3P)5d\ ^2P_{1/2}$	25.053	25.06	25.05	
12	25.186	25.187	$(^3P)5d\ ^2D_{3/2}$	25.183		25.18	
13	25.265	25.266	$(^3P)5d\ ^4P_{1/2}$	25.265	25.27	25.26	
14	25.332[a]	25.331	$(^3P)5d\ ^4F_{5/2}$	25.334			
15	25.384[a]	25.385	$(^3P)6s\ ^2P_{1/2}$	25.395	25.39	25.38	
16	25.443	25.444	$(^3P)5d\ ^4F_{3/2}$				
17	25.508	25.509	$(^3P)5d\ ^4P_{3/2}$			25.51	
18	25.522[a]	25.521	$(^3P)5d\ ^4P_{5/2}$	25.521	25.52		
19	25.573	25.573	$(^3P)5d\ ^4F_{7/2}$				
20	25.713	25.714	$(^1D)6s\ ^2D_{5/2}$	25.715	25.71	25.73	
21	25.932	25.933	$(^3P)5d\ ^2P_{3/2}$	25.937		25.92	
22	25.991	25.991	$(^3P)6p\ ^4P_{3/2}$	25.990			
23	26.010	26.011	$(^3P)6p\ ^4P_{5/2}$				
24	26.102	26.104	$(^3P)5d\ ^2F_{5/2}$	26.105			
25	26.131	26.131	$(^1D)6s\ ^2D_{3/2}$	26.132	26.12	26.12	
26	26.205	26.204	$(^3P)6p\ ^2D_{5/2}$	26.216			
27	26.228[a]	26.224	$(^3P)6p\ ^2P_{1/2}$				
		26.228	$(^3P)6p\ ^4D_{7/2}$				
28	26.356	26.357	$(^3P)5d\ ^2D_{5/2}$	26.374	26.37	26.36	
29	26.376	26.377	$(^1D)5d\ ^2G_{9/2}$				
		26.378	$(^1D)5d\ ^2G_{7/2}$				
30	26.609	26.609	$(^3P)6p\ ^2P_{3/2}$	26.609	26.61	26.61	
31	26.894	26.895	$(^1D)5d\ ^2F_{5/2}$	26.895	26.90	26.88	
32	27.059	27.060	$(^3P)6p\ ^4D_{1/2}$	27.040		27.05	
33	27.114	27.114	$(^1D)5d\ ^2F_{7/2}$	27.112	27.11		
34	27.154	27.154	$(^3P)6p\ ^4P_{1/2}$			27.14	
35	27.209[a]	27.210	$(^3P)6p\ ^4D_{3/2}$	27.213	29.29	27.20	
36	27.391	27.394	$(^3P)6p\ ^4D_{5/2}$				
37	27.412[a]	27.412	$(^3P)6p\ ^4S_{3/2}$	27.414	27.42	27.42	
38	27.509	27.513	$(^1D)5d\ ^2P_{3/2}$				
39	27.538	27.540	$(^3P)6p\ ^2D_{3/2}$	27.539	27.54	27.53	
		27.542	$(^1D)5d\ ^2D_{5/2}$				
40	27.573	27.575	$(^3P)6p\ ^2S_{1/2}$				
41	27.877	27.878	$(^1D)5d\ ^2P_{1/2}$	27.877	27.88	27.87	
42	27.941	27.941	$(^1D)5d\ ^2D_{3/2}$	27.942	27.97		
43	28.108	28.108	$(^1D)6p\ ^2F_{5/2}$	28.107			
44	28.153	28.155	$(^1S)6s\ ^2S_{1/2}$	28.153	28.16		
45	28.204	28.207	$(^1D)6p\ ^2P_{3/2}$	28.207	28.22	28.19	

Table 3. Continued.

	This work	Hansen and Persson (1987)		Carlsson-Göthe *et al* (1991)	Kikas *et al* (1996)	Hall *et al* (1990)	Shiell *et al* (1999)
	Energy (eV)	Energy (eV)	Assignments	Energy (eV)	Energy (eV)	Energy (eV)	Energy (eV)
46	28.255	28.256	$(^1D)6p\ ^2F_{7/2}$	28.260		28.25	
47	28.487	28.487	$(^1D)6p\ ^2D_{3/2}$	28.488	28.51		
48	28.522	28.522	$(^1D)6p\ ^2D_{5/2}$				
49	28.560	28.560	$(^3P)7s\ ^4P_{5/2}$				
50	28.588	28.588	$(^1D)6p\ ^2P_{1/2}$	28.589	28.60	28.58	
51	28.642	28.643	$(^3P)7s\ ^2P_{3/2}$			28.63	
52	28.876	28.876	$(^1D)5d\ ^2S_{1/2}$	28.885	28.88	28.89	
53	28.935	28.931	$(^3P)6d\ ^4D_{7/2}$				
		28.936	$(^3P)6d\ ^4D_{5/2}$				
54	28.957	28.956	$(^3P)6d\ ^4D_{3/2}$				
55	29.007	29.006	$(^3P)6d\ ^4F_{9/2}$				
56	29.062	29.061	$(^3P)6d\ ^2P_{1/2}$	29.062	29.07	29.06	
		29.063	$(^1S)5d\ ^2D_{5/2}$				
		29.066	$(^3P)6d\ ^2F_{7/2}$				
57	29.247	29.248	$(^1S)5d\ ^2D_{3/2}$			29.24	
58	29.330	29.330	$(^3P)6d\ ^4P_{1/2}$		29.34	29.35	
59	29.375	29.376	$(^3P)6d\ ^2D_{5/2}$	29.371			
		29.380	$(^3P)7p\ ^4D_{5/2}$				
60	29.444	29.443	$(^3P)6d\ ^4P_{3/2}$	29.447	29.45		
		29.444	$(^3P)7p\ ^4P_{5/2}$				
61	29.492	29.492	$(^3P)4f\ ^4P_{7/2}$				
62	29.514	29.511	$(^3P)4f\ ^4P_{1/2}$		29.52		
		29.514	$(^3P)4f\ ^4P_{5/2}$				
63	29.599	29.597	$(^3P)7s\ ^4P_{1/2}$	29.612			
64	29.609	29.611	$(^3P)7p\ ^4P_{3/2}$		29.61		
65	29.790	29.783	$(^3P)7s\ ^4P_{3/2}$				

[a] Resonance observed on the high-energy side of the threshold peak (see table 4).

apparently do not decay to the lower-energy satellite states but were nevertheless assumed to enhance the ionic states with thresholds above 30 eV. The observed ‘tail’ also implies that the partial cross section of the $(^3P)5p\ ^2P^o_{1/2,3/2}$ states must rise *very* steeply from threshold (for a similar example in argon see Cvejanović and Reddish (1995)). Similarly, the resonance features between 31.7 and 32 eV are considered to be coupled to the nearest, lower-energy ionic state(s), which happens to include the other odd-parity doublet states: $(^3P)5p\ ^2S^o_{1/2}/^2D^o_{3/2}$. Both Codling and Madden (1972) and Hall *et al* (1990) have also observed these resonances and identified them as belonging to the $(^1S)5sn p\ ^2S_{1/2}$ series whose limit has been determined optically to be 32.075 eV. The threshold yield at that energy location is highly structured, possibly due to strong resonant coupling to the states above the ^2S threshold and a partially resolved contribution just below at 32.053 eV. This latter feature and the sharp threshold peak at 31.944 eV have not been observed in previous studies. They could be associated with the $(^1D)4d\ ^2G$ or ^2F states which are missing from the optical data but may be in this energy region. The corresponding $(^1D)5d$ states have, however, been identified (see Minnhagen *et al* 1968). This intriguing energy region, with its surprisingly strong resonance presence, would be an appropriate topic for further experimental and theoretical studies.

3.2. Xenon

The threshold photoelectron spectrum of xenon (see figures 3 and 5), taken with similar spectrometer tuning to that of krypton, covered a more extensive photon energy range, stretching well into the double-ionization region. Virtually all the ionic states below 30 eV have been observed (see table 3) and there are only a few significant shoulders on the high-energy sides of the threshold peaks (see table 4), indicating that the threshold tuning was even more selective than for krypton. The most intense threshold peaks are $(^3P)5d\ ^4D_{5/2,7/2}$ (23.957 eV), $(^3P)6s\ ^4P_{1/2}$ (24.671 eV) and $(^1D)5d\ ^2P_{1/2}$ (27.877 eV). As noted above, the corresponding $(^3P)5s\ ^4P_{1/2}$ state in krypton also had a strong threshold peak, but the intensities for the other corresponding states were not particularly notable. This is not a surprise, however, as coupling to resonance channels (as observed in TPES) depends not only on angular momentum considerations, but on energy proximity as well, making a direct comparison between the two gases difficult. Nevertheless, the $(^3P)6s\ ^4P_{1/2}$ threshold peak has probably been influenced by a nearby resonance at 24.69 eV, identified as number 91 by Codling and Madden (1972) (see table 4).

Table 4. Observed resonances in the threshold photoelectron spectrum of xenon of figure 3.

This work	Codling and Madden (1972)	
Energy (eV)	Energy (eV)	No
24.05		
24.15	24.156	78
24.69	24.692	91
25.35	25.345	113
25.40	25.395	116
	25.410	117
25.54	25.535	122
26.24	26.248	138
27.23	27.225	165
27.43	27.427	174

Despite the differences in energy resolution, we can make a comparison of the threshold intensities observed by two different techniques: PFI-ZEKE (Shiell *et al* 1998, 1999) and conventional TPES. In doing so, one makes the obvious assumption that the detection efficiencies in both methods are constant at all photon energies. Figure 4 shows the histogram of relative intensities for the ten resolved peaks below 25 eV as obtained by the two techniques. While it is tempting to normalize their yields on the single-hole $^2S_{1/2}$ state, the asymmetric profile of its peak in the TPES spectrum indicates likely resonant enhancement. This raises the question of how to normalize the data from the two methods. One can suggest reasons why the PFI-ZEKE yield could be *less* than the 'true' threshold photoionization cross section, namely that the intermediate high-n Rydberg states either fluorescence or (more likely) autoionize (producing fast electrons) prior to the field-ionizing pulse, but it is hard to identify mechanisms which would give relatively *more* yield for PFI-ZEKE than TPES. Consequently, *if* the TPES yield for a particular state was relatively *lower* than that of PFI-ZEKE, this would imply that the 'above'-threshold resonances contributing to the TPES signal have *destructively* interfered with the direct photoionization mechanism. However, this seems unlikely for quartet states, as generally there would be little direct excitation with which to interfere. A comparison of the PFI-ZEKE and TPES spectra indicate that the $(^3P)6s\ ^4P_{5/2}$ state at 23.669 eV shows relatively more yield (compared with neighbouring states) in the PFI-ZEKE method than in

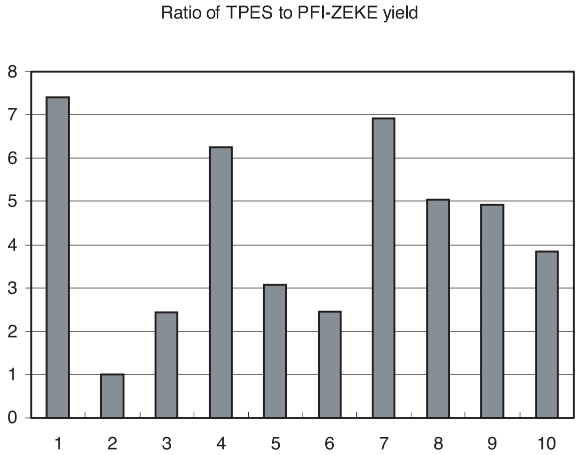

Number	Assignment
1	$5s5p^6\ ^2S_{1/2}$
2	$(^3P)\ 6s\ ^4P_{5/2}$
3	$(^3P)\ 6s\ ^2P_{3/2}$
4	$(^3P)\ 5d\ ^4D_{5/2}$
	$(^3P)\ 5d\ ^4D_{7/2}$
5	$(^3P)\ 5d\ ^4D_{3/2}$
6	$(^3P)\ 5d\ ^4D_{1/2}$
7	$(^3P)\ 5d\ ^4F_{9/2}$
8	$(^3P)\ 6s\ ^4P_{1/2}$
9	$(^3P)\ 5d\ ^2F_{7/2}$
10	$(^3P)\ 6s\ ^4P_{3/2}$

Figure 4. A histogram of the relative intensities of 11 ionic states of xenon obtained by the PFI-ZEKE (Shiell *et al* 1999) and TPES methods. The state numbering corresponds to that of table 3. The relative intensities of this study are normalized at peak 2 for reasons given in the text. The general relative enhancement of the TPES method is a measure of the resonant contribution to the near-threshold yield.

TPES. Consequently, for the reasons outlined above, this state was chosen for normalizing the relative yields from the two techniques in figure 4. Remarkably, the other states all show TPES-to-PFI-ZEKE yield ratios which are significantly greater than 1. Other than the $^2S_{1/2}$ state, the highest ratios (~ 7) occur with the highest J values and the average enhancement is about a factor of four. The precise reasons for such profound differences in the ratios and their variations with assignment are not clear. In order to investigate further the indicated enhancement of the photoabsorption when ionic state thresholds are crossed one will need to have similar ΔE detection bandwidths for the two methods. This requires the use of third-generation synchrotron sources with a well tuned penetrating field threshold analyser.

As expected, the threshold yield above 30 eV becomes progressively weaker. Consequently, the spectrum in figure 5 suffers from a relatively poor signal-to-noise ratio, but is shown as it covers the energy region of the lowest Xe^{2+} states. As in the case of krypton, one has to consider the possible effects of contamination by higher-order light. Second-order light would produce threshold peaks in the 32.5–35 eV region with the strongest sharp shake-off peak at 32.55 eV and with broad peaks, corresponding to the PCI-shifted $4d^{-1}$ states, at ~ 33.9 and ~ 34.9 eV (Heimann *et al* 1987, Avaldi *et al* 1991). There is no clear evidence of second-order structure in the xenon spectrum of figure 5; indeed third-order radiation is deemed to be a greater problem (by a factor of ~ 3) on this beamline at the photon energies covered in this study.

The most intense, resolved features are listed in table 5 and assignments, where known, are also given. The LS-coupling scheme is progressively less appropriate in this energy region and Hansen and Persson (1987) abandon its use for the odd-parity states in favour of the jK-coupling scheme. In this energy region there is a high density of states, many of which are not resolved, or observed, in this study. Where there is ambiguity in the assignments only the basic configuration is identified in table 5. It is interesting to note that the strong threshold peak at 30.78 eV, which is also observed in the other PES studies, remains unassigned. Above 32 eV there are no optical data with which to compare, although many states have been observed in the various photoelectron studies. The tentative assignments, which focus on the Rydberg

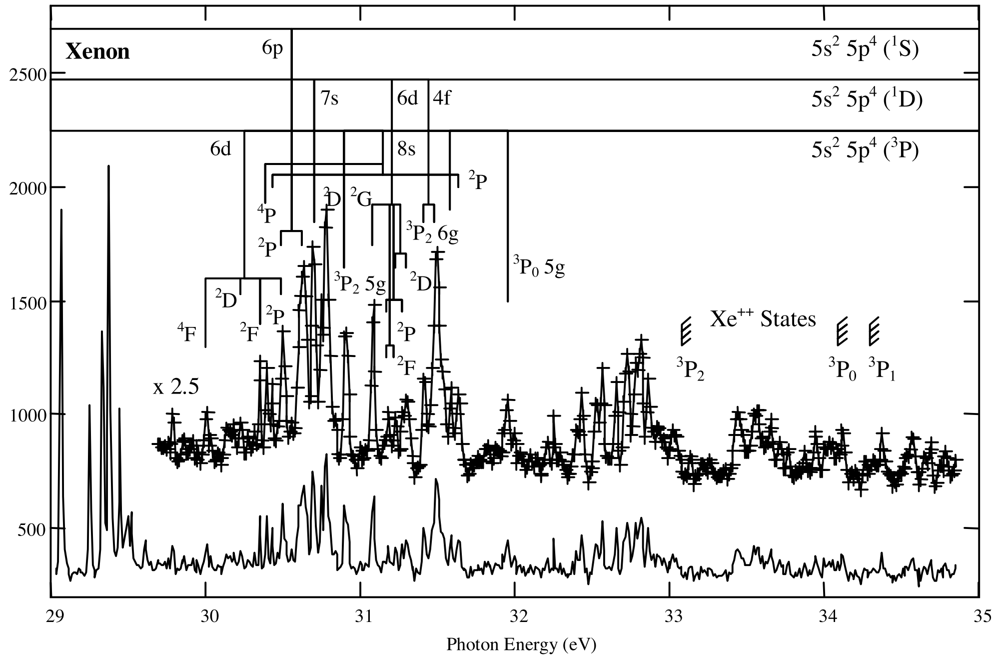

Figure 5. The threshold photoelectron spectrum of xenon taken with photon energy increments of 10 meV and an accumulation time of 10 s/point. Note the threshold yield, y-scale, has an offset of 200 counts. The lower curve shows the raw data and the inserted spectrum (scale $\times 2.5$) has been smoothed slightly to highlight the main features. The ionic state assignments below 32 eV are from Hansen and Persson (1987); note that not all the multiplet members have been observed (see table 5 for details). The energies of the lowest double-ionization thresholds are also indicated.

series associated with the ^{1}D and ^{1}S core, are also compared in table 5. Even so, many more states have been observed than identified and the quality of the data in this energy region could allow for other assignments.

Our measurements above 30 eV generally confirm the previously seen peaks and also show others despite the relatively poor signal-to-noise ratio. The number of overlapping Rydberg series, each with its different quantum defect, along with the various possible Xe^{2+} states makes an analysis of this region extremely difficult. An overview of the threshold spectrum reveals a variety of resolved (and assigned) peaks between ~ 30.5 and ~ 31.5 eV, followed by distinct clusters at progressively narrower energy intervals as well as energy extent (i.e. at ~ 32.4–33.1, ~ 33.4–33.8, ~ 34.0–34.2 eV) which then merge to asymmetric peaks above 34.5 eV. The convergence of the features above 34 eV suggests a predominance of ^{1}D Rydberg series in this region (whose limit is at 35.20 eV), which is further supported by the many ^{1}D states identified in the 30.7–31.5 eV region (see table 5). The apparent peaks above 34 eV should then be interpreted as different n values of the various Rydberg series (i.e. averaged over all quantum defects) rather than a particular series. The dominance of the 6d and 7s configuration between 30.7 and 31.5 eV indicates an overall Rydberg series of even parity. A number of ^{3}P states have also been identified between 30.5 and 31.5 eV, generally of high orbital angular momentum (i.e. f, g). The series of features between 31.9 and 33 eV are overlapping Rydberg states converging to the Xe^{2+} $^3P_2$ limit at 33.08 eV, which one should note is twice as intense as the $^3P_{0,1}$ and ^{1}D Xe^{2+} states (and ~ 20 times stronger than the Xe^{2+} ^{1}S state at 37.56 eV) as observed by threshold photoelectron coincidence spectroscopy (see Hall *et al* 1992a, b). It is

Table 5. The energies and assignments of the ionic states in xenon between 30.0 and 34.8 eV.

	This work	Hansen and Persson (1987)		Carlsson-Göthe *et al* (1991)	Kikas *et al* (1996)	
	Energy (eV)	Energy (eV)	Assignment	Energy (eV)	Energy (eV)	Assignment[a]
66	30.00	30.001	$(^3P)6d\ ^4F_{3/2}$			
67	30.23	30.224	$(^3P)6d\ ^2D_{3/2}$			
68	30.35	30.347	$(^3P)6d\ ^2F_{5/2}$	30.348	30.37	
69	30.39	30.394	$(^3P)8s\ ^4P_{5/2}$			
70	30.43	30.420	$(^3P_0)4f[3]_{5/2}$[d]	30.424		
		30.426	$(^3P)8s\ ^2P_{3/2}$			
		30.426	$(^3P_0)4f[3]_{7/2}$[d]			
71	30.49	30.490	$(^3P)6d\ ^2P_{3/2}$	30.502	30.50	
		30.507	$(^1S)6p\ ^2P_{1/2}$			
72	30.61	30.598	$(^3P_1)4f[2]_{5/2}$[d]			
73	30.63[c]	30.627	$(^1S)6p\ ^2P_{3/2}$	30.635	30.64	
		30.638	$(^3P_1)4f[4]_{7/2}$[d]			
74	30.70[c]	30.690	$(^1D)7s\ ^2D_{5/2}$		30.68	
		30.703	$(^1D)7s\ ^2D_{3/2}$			
75	30.74[c]	30.740	$(^3P_2)5f[5]_{11/2}$[d]			
		30.754	$(^3P_2)5f[5]_{9/2}$[d]			
76	30.78			30.773	30.78	
77	30.90[c]	30.910	$(^3P_2)5g$[d]	30.910	30.89	
78	31.08[c]	31.076	$(^1D)6d\ ^2G_{9/2}$	31.063	31.09	
79	31.18	31.172	$(^1D)6d\ ^2P_{3/2}$	31.166	31.16	
		31.172	$(^1D)6d\ ^2F_{5/2}$			
80	31.23	31.221	$(^1D)6d\ ^2F_{7/2}$			
		31.228	$(^1D)6d\ ^2D_{5/2}$			
81	31.28	31.271	$(^1D)6d\ ^2P_{1/2}$		31.29	
82	31.30	31.299	$(^1D)6d\ ^2D_{3/2}$	31.302		
83	31.41	31.405	$(^1D_2)4f[1]_{3/2}$[d]	31.400	31.42	
		31.451	$(^3P_2)6f[5]_{11/2,9/2}$[d]	31.450		
84	31.49[c]	31.488	$(^1D_2)4f[5]_{11/2}$[d]	31.496	31.50	$(^1D)6d\ ^2S$
85	31.53	(31.509)	$(^1D_2)4f[2]_{3/2}$[d]			
86	31.58	31.584	$(^3P_2)6g$[d]		31.59	$(^3P)8s\ ^4P$
		31.607	$(^3P)8s\ ^4P_{3/2}$	31.610		$(^1D)4f\ ^4P$
		31.608	$(^1D_2)4f[3]_{7/2}$[d]			
87	31.64	31.641	$(^3P)8s\ ^2P_{1/2}$		31.64	
		31.84	$(^3P)7d\ ^2P$		31.85	
88	31.95	31.920	$(^3P_0)5g$[d]	31.952	31.95	$(^3P)7d\ ^4D$
89	31.99	31.988	$(^3P_2)7g$[d]		32.03	
90	32.25			32.211	32.22	
91	32.40			32.415	32.41	
92	32.44					
93	32.53			32.535	32.55	
94	32.56					
95	32.65					
96	32.72	32.7	$(^3P)8d\ ^4D$		32.74	
97	32.78					
98	32.82			32.811	32.83	$(^1D)7d\ ^2S$
99	32.86	32.85	$(^1D)7d\ ^2P$		32.89	$(^1D)7d\ ^2P$[b]
		32.91	$(^1D)7d\ ^2S$			
100	33.02				32.98	

Table 5. Continued.

	This work	Hansen and Persson (1987)		Carlsson-Göthe *et al* (1991)	Kikas *et al* (1996)	
	Energy (eV)	Energy (eV)	Assignment	Energy (eV)	Energy (eV)	Assignment[a]
101	33.04	33.04	$(^1S)7s\ ^2S$		33.08	$(^1S)7s\ ^2S$
				33.180	33.15	
					33.31	
102	33.43			33.440	33.43	
103	33.54					
104	33.57	33.6	$(^1D)8d\ ^2S$	33.557	33.56	
105	33.65			33.641	33.63	
106	33.71	33.7	$(^1D)8d\ ^2P$	33.728		
107	33.77				33.81	$(^1D)8d\ ^2S$
108	33.87			33.892		
109	33.94				33.92	
110	34.00					
111	34.03			34.030	34.03	$(^1D)9d\ ^2S$
112	34.06					
113	34.09				34.09	
114	34.12			34.165		
115	34.38			34.320	34.38	$(^1D)10d\ ^2S$
				34.507		
116	34.57			34.577	34.54	
117	34.69			34.648	34.69	
118	34.78			34.750		

[a] Assignments where different from Hansen and Persson (1987).
[b] Assignment from Whitfield *et al* (1994).
[c] Threshold peak also observed by Hall *et al* (1990).
[d] Assignment in jK notation.

likely, then, that the features near 33.5 eV contain corresponding series converging to the Xe^{2+} $^3P_{0,1}$ states at 34.09 and 34.29 eV, but possible contamination due to second-order light cannot be excluded totally. Clearly, a more comprehensive study of this energy region will require higher photon resolution, with significantly better signal-to-noise ratio and the rejection of higher-order light.

4. Summary

Threshold photoelectron spectra for krypton and xenon have been measured and many previously unresolved states have been observed and identified. In the case of krypton, there are a few cases where a resonance contribution is clearly observed and these generally involve a significant change in the angular momentum configuration of both the outer electrons and the ion core. As such, they provide a clear demonstration of many-body processes in photoionization. A more extensive energy range was covered in this TPES study of xenon and a comparison of the photoionization yield at threshold taken by two distinctly different, yet complementary experimental detection techniques was made for the first time. Although there were only PFI-ZEKE data for ten states, the comparison has shown a remarkable enhancement of the TPES yield relative to the PFI-ZEKE measurements. This TPES study of Kr and Xe confirms and extends the spectroscopic data for these ion states and highlights regions of interest for future work on third-generation synchrotron sources.

Acknowledgments

We wish to thank EPSRC for its continued support for this project. We would also like to thank the Leverhulme Trust for a Fellowship for SC and Newcastle University for the Ridley Fellowship for JPW.

References

Avaldi L, Hall R I, Dawber G, Rutter P M and King G C 1991 *J. Phys. B: At. Mol. Opt. Phys.* **24** 427–38
Becker U and Shirley D A 1990 *Phys. Scr.* T **31** 56–66
Carlsson-Göthe M, Baltzer P and Wannberg B 1991 *J. Phys. B: At. Mol. Opt. Phys.* **24** 2477–85
Codling K and Madden R P 1972 *J. Res. Natl Bur. Stand.* A **76** 1–12
Čubrić D, Wills A A, Comer J and MacDonald M A 1992 *J. Phys. B: At. Mol. Opt. Phys.* **25** 5069–83
Cvejanović S, Bagley G W and Reddish T J 1994 *J. Phys. B: At. Mol. Opt. Phys.* **27** 5661–79
Cvejanović S and Read F H 1974 *J. Phys. B: At. Mol. Phys.* **7** 1180–93
Cvejanović S and Reddish T J 1995 *J. Phys. B: At. Mol. Opt. Phys.* **28** L1–7
Ehresmann A, Vollweiler F, Schmoranzer H, Sukhorukov V L, Lagutin B M, Petrov I D, Mentzel G and Schartner K H 1994 *J. Phys. B: At. Mol. Opt. Phys.* **27** 1489–96
Hall R I, Avaldi L, Dawber G, Zubek M and King G C 1990 *J. Phys. B: At. Mol. Opt. Phys.* **23** 4469–85
Hall R I, Dawber G, McConkey A G, MacDonald M A and King G C 1992a *Z. Phys.* D **23** 377–81
Hall R I, McConkey A, Ellis K, Dawber G, MacDonald M A and King G C 1992b *J. Phys. B: At. Mol. Opt. Phys.* **25** 799–810
Hansen J E and Persson W 1987 *Phys. Scr.* **36** 602–43
Heimann P A *et al* 1987 *J. Phys. B: At. Mol. Phys.* **20** 5005–22
Jureta J, Cvejanović S, Brunt J N H and Read F H 1978 *J. Phys. B: At. Mol. Phys.* **11** L347–51
Kikas A, Osborne S J, Ausmees A, Svensson S, Sairanen O-P and Aksela S 1996 *J. Electron Spectrosc. Relat. Phenom.* **77** 241–66
Krause M O, Whitfield S B, Caldwell C D, Wu J-Z, van der Meulen P, de Lange C A and Hansen R W C 1992 *J. Electron Spectrosc. Relat. Phenom.* **58** 79–104
Lagutin B M, Petrov I D, Sukhorukov V L, Whitfield S B, Langer B, Viefhaus J, Wehlitz R, Berrah N, Mahler W and Becker U 1996 *J. Phys. B: At. Mol. Opt. Phys.* **29** 937–76
Lagutin B M, Sukhorukov V L, Petrov I D, Schmoranzer H, Ehresmann A and Schartner K H 1994 *J. Phys. B: At. Mol. Opt. Phys.* **27** 5221–39
Minnhagen L, Strihed H and Peterssen B 1968 *Ark. Fys.* **39** 471–93
Moore C E 1952 *Atomic Energy Levels (NBS Circular)* vol 2 (Washington, DC: US Govt Printing Office)
——1958 *Atomic Energy Levels (NBS Circular)* vol 3 (Washington, DC: US Govt Printing Office)
Reddish T J, Richmond G, Bagley G W, Wightman J P and Cvejanović S 1997 *Rev. Sci. Instrum.* **68** 2685–92
Schmoranzer H, Ehresmann A, Vollweiler F, Sukhorukov V L, Lagutin B M, Petrov I D, Schartner K H and Möbus B 1993 *J. Phys. B: At. Mol. Opt. Phys.* **26** 2795–810
Shiell R C, Evans M, Stimson S, Hsu C-W, Ng C Y and Hepburn J W 1998 *Phys. Rev. Lett.* **80** 472–5
——1999 *Phys. Rev.* A **59** 2903–9
Sukhorukov V L, Lagutin B M, Petrov I D, Schmoranzer H, Ehresmann A, Vollweiler F and Schartner K H 1995 *J. Electron Spectrosc. Relat. Phenom.* **76** 421–6
Svensson S, Eriksson B, Mårtensson N, Wendin G and Gelius U 1988 *J. Electron Spectrosc.* **47** 327–84
Whitfield S B, Langer B, Viefhaus J, Wehlitz R, Berrah N, Mahler W and Becker U 1994 *J. Phys. B: At. Mol. Opt. Phys.* **27** L359–66
Wills A A, Cafolla A A and Comer J 1990 *J. Phys. B: At. Mol. Opt. Phys.* **23** 2029–36